Bone 123 (2019) 246–259

Contents lists available at ScienceDirect

Bone

journal homepage: www.elsevier.com/locate/bone

Full Length Article

Aging of mouse intervertebral disc and association with back pain

Kathleen Vincent[a], Sarthak Mohanty[a], Robert Pinelli[a], Raffaella Bonavita[a], Paul Pricop[a], Todd J. Albert[a,c], Chitra Lekha Dahia[a,b,*]

[a] Hospital for Special Surgery, New York, NY 10021, USA
[b] Department of Cell and Developmental Biology, Weill Cornell Medicine, Graduate School of Medical Science, New York, NY 10065, USA
[c] Weill Cornell Medical College, New York, NY 10065, USA

ARTICLE INFO

Keywords:
Low back pain
Aging
Intervertebral disc degeneration
Mouse model
Molecular pain

ABSTRACT

With the increased burden of low back pain (LBP) in our globally aging population there is a need to develop preclinical models of LBP that capture clinically relevant features of physiological aging, degeneration, and disability. Here we assess the validity of using a mouse model system for age-related LBP by characterizing aging mice for features of intervertebral disc (IVD) degeneration, molecular markers of peripheral sensitization, and behavioral signs of pain. Compared to three-month-old and one-year-old mice, two-year-old mice show features typical of IVD degeneration including loss of disc height, bulging, innervation and vascularization in the caudal lumbar IVDs. Aging is also associated with the loss of whole-body bone mineral density in both male and female mice, but not associated with percent lean mass or body fat. Additionally, two-year-old mice have an accumulation of TRPA1 channels and sodium channels $Na_V1.8$ and $Na_V1.9$ in the L4 and L5 lumbar dorsal root ganglia consistent with changes in nociceptive signaling. Lastly, the effect of age, sex, and weight on mobility, axial stretching and radiating pain measures was assessed in male and female mice ranging from two months to two years in a general linear model. The model revealed that regardless of sex or weight, increased age was a predictor of greater reluctance to perform axial stretching and sensitivity to cold, but not heat in mice.

1. Introduction

Despite improvements in life expectancy worldwide [1], the prevalence of low back pain (LBP) continues to increase [2,3] and as of 2013 is the third most costly health care condition in the US [4]. One age-related risk factor for LBP is the presence of degenerative changes in the spine, and specifically the intervertebral disc (IVD) [5]. The IVD is a hydrated structure forming a junction between adjacent vertebrae and is essential for the mobility and support of the spine. At its core, the IVD contains a semi-liquid nucleus pulposus (NP) which is surrounded by layers of fibrocartilaginous annulus fibrosus (AF), nested between cartilaginous endplates (EP). As a result of physiological aging, the structural integrity of the IVD becomes increasingly compromised [6,7]. While there is a clear association between IVD degeneration and LBP, not all cases of degeneration are painful [5], making it necessary to distinguish painful from innocuous IVD degeneration.

To better characterize the initiation and progression of LBP, numerous preclinical models have been developed, and their advantages and limitations reviewed extensively [8–12]. Mechanical injury-based models include damaging the lumbar IVD [13–15], facet joints [16], displacement of the nerve roots [17], or compression in the nerve roots [18] and dorsal root ganglia (DRG) [19,20]. These models recreate painful syndromes that capture functional impairments found in LBP, such as altered gait [14,21], grooming [14], thermal hyperalgesia [17,20], pressure algometry [15], or mechanical allodynia [16,17,20,22]. Related to these models are the chemically-induced models of LBP. These models recapitulate inflammatory features of LBP by exposing the lumbar DRG to the NP and other pro-inflammatory mediators resulting in reduced, though transient, mechanical thresholds [23–26], without causing mechanical damage to the spine. Models targeting DRGs have the additional advantage of producing allodynia and hyperalgesia specific to the ipsilateral hind paw making it possible to infer causal relationships between injury site and pain outcomes [17,19,20,23]. These models, while providing a guide for rapid onset LBP due to disease or injury, may diverge mechanistically from LBP developed over the course of aging. The sand rat (*Psammomys obesus*) is a widely used model for spontaneous disc degeneration [27]. These animals display disc wedging, disc narrowing, and endplate

Abbreviations: LBP, low back pain; IVD, intervertebral disc; MFI, mean fluorescent intensity; NP, nucleus pulposus; AF, annulus fibrosus; EP, endplate; DRG, dorsal root ganglia; OFT, open field test; TST, tail suspension test; DEXA, dual energy X-ray absorptiometry; DHI, disc height index

* Corresponding author at: 535 East 70th Street, New York, NY 10021, USA.
E-mail address: dahiac@hss.edu (C.L. Dahia).

https://doi.org/10.1016/j.bone.2019.03.037
Received 15 October 2018; Received in revised form 26 February 2019; Accepted 26 March 2019
Available online 29 March 2019
8756-3282/

calcification by two to six months of age [28] and have similar BDNF patterning in the AF as degenerated human IVDs [29]. It remains to be tested, however, whether the degenerative changes are painful in these animals.

Capturing features of LBP more relevant to aging patients, genetic models of IVD degeneration produce progressive, painful disorders. These genetic models rely on the global knockout of critical matricellular proteins including type IX collagen [30–32], type II A1 collagen [33], and SPARC [34–38] to accelerate disc degeneration phenotypes. The premature degeneration of the discs in these genetic models is associated with behavioral changes associated with pain such impaired grip strength [34], mechanical allodynia [31,39], cold allodynia [34,35,37–39], reduced mobility [33,35], and measures of axial discomfort [34,35,37,38]. An advantage to these models is the inclusion of non-mutant control mice who also exhibit changes with age. Compared to three-month-old mice, 15-month-old mice run shorter distances [33,40] and 20-month-old mice are more sensitive to cold but not mechanical stimuli [35]. These studies suggest that certain pain-related behaviors appear over the course of physiological aging and will appear earlier in genetic models. However, these pain behaviors cannot be ascribed to IVD degeneration specifically as the loss of type IX collagen and reduction of type II A1 collagen in articular cartilage leads to osteoarthritic phenotypes [30,40,41] and SPARC null mice develop osteopenia [42]. In addition, pain in these mice could be due to uncharacterized degenerative changes in other joints or tissues in the body that may be affected by the loss of these matricellular proteins.

One of the difficulties in assessing LBP in animal model systems is capturing clinically relevant features of pain. Reflexive behaviors, such at the tail flick or paw withdrawal thresholds are replicable, but are argued to have less relevance to the clinical symptoms of chronic pain [43]. Evoked pain behaviors, such as nocifensive responses to noxious stimuli, and functional impairments, such as gait analysis, may capture more pertinent features of LBP. Elderly patients with LBP have an increased fear of movement [44], and unsurprisingly spend less time walking [45], have altered stride patterns [46], and reduced range of motion in lower extremities compared to patients without LBP [47]. As such, animal models characterized by functional impairments may represent a more reliable tool for developing therapeutics by reflecting symptoms reported in the clinical population.

Understanding LBP and painful IVD degeneration in the context of aging in animal models, and how they compare to human pathophysiology, may serve to improve prognosis and management of LBP in older adults. The objective of the present investigation is to provide a description of behavioral features and molecular changes associated with back pain and disc degeneration in a physiologically aging mouse model system. Specifically, we aim to characterize aging body composition and IVD morphology in mice in the absence of injury, correlate mobility and radiating pain to age and sex in these mice, and quantify sodium channel accumulation in the lumbar DRGs for signs of peripheral sensitization. These results will indicate how well mice may serve as a proxy for human disc degeneration, and provide a foundation upon which future LBP and IVD degeneration mouse model systems may build.

2. Methods

2.1. Mice

All mice were maintained in accordance with the National Institutes of Health Guide for the Care and Use of Laboratory Animals, and all experiments were carried out in strict accordance with institutional guidelines under Institutional Animal Care and Use Committee (IACUC) approved at Weill Cornell Medical College (WCMC). IACUC at WCMC approved the study described in this manuscript with Animal Use Protocol number 2016-0026. Animals were housed in a facility with 12:12 light-dark cycle with food given *ad libitum*. Mice used were based on a C57BL/6J or FVB background that were either wild type or contained transgenes (Supplemental Table 1) that have no impact on the IVD structure and pain measures taken for this study.

2.2. Radiography and DEXA scans

Radiographs and dual energy X-ray absorptiometry (DEXA) scans were collected using the UltraFocus high resolution digital X-ray cabinet by Faxitron Bioptics, LLC (Arizona, USA). Prior to imaging, automatic calibration and automatic exposure control was used to select the appropriate exposure time and kV settings for the samples. Mice were anesthetized with 2% isoflurane and placed in the X-ray chamber on their ventral side with all limbs extended away from midline in a natural position to obtain whole body DEXA and coronal radiographic images. Mice were then moved to lie on their side in a natural position with tail extended to obtain sagittal radiographic images. DEXA data regarding mouse bone mineral density (BMD), body fat weight, lean muscle mass and total weight was exported for analysis. Percent body fat and percent lean muscle mass were calculated as follows:

$$\%body\ fat = 100 \times \frac{body\ fat\ mass\ (g)}{totalweight\ (g)}$$

$$\%bodymuscle = 100 \times \frac{leanmusclemass\ (g)}{totalweight\ (g)}.$$

In total, 97 mice (46 females) between the ages of three to 21 months were used for DEXA analyses. Using the UltraFocus measuring tools, disc height index (DHI) for L3 to S1 IVDs was measured by averaging measurements from the anterior, middle, and posterior portions of the IVD from a sagittal plane and dividing it by the average measurements of the anterior, middle, and posterior portions of the adjacent vertebral bones (illustrated in Fig. 2F) [48]. A total of 25 mice (13 female) were used for DHI analyses.

2.3. Behavioral testing

222 mice between the ages of two and 24 months of age and of both sexes were used for behavioral testing (Table 1). All behavioral tests were carried out during the light cycle between the hours of 9:00 am and 5:00 pm. Mice were habituated to the testing room in their home cage for 30 min prior to testing. Each mouse was weighed on the day tested. No breeding, pregnant or nursing mice were used for behavioral experiments. The open field test, tail suspension test and acetone test were all performed in the same order on the same day with a 20-minute rest period between successive tests. The capsaicin test was always performed on the next day. After each behavioral assay, mice were placed alone in a holding cage until all mice had completed the tests. Real-time scoring was performed by the experimenter in the room and a second scoring was obtained from video recording by an experimenter blind to the date of testing, age, sex, strain and weight of the mouse. An average of the two scores was obtained and used for analysis.

Table 1
Mouse demographics by age and sex.

Age (months)	# mice	# female mice (%)	
2	16	7	(44)
4	14	9	(64)
6	15	7	(47)
8	26	12	(46)
10	20	11	(55)
12	19	6	(32)
14	36	10	(28)
16	12	4	(33)
18	15	8	(53)
20	14	9	(64)
22	14	8	(57)
24	21	12	(57)
Total	222	103	(46)

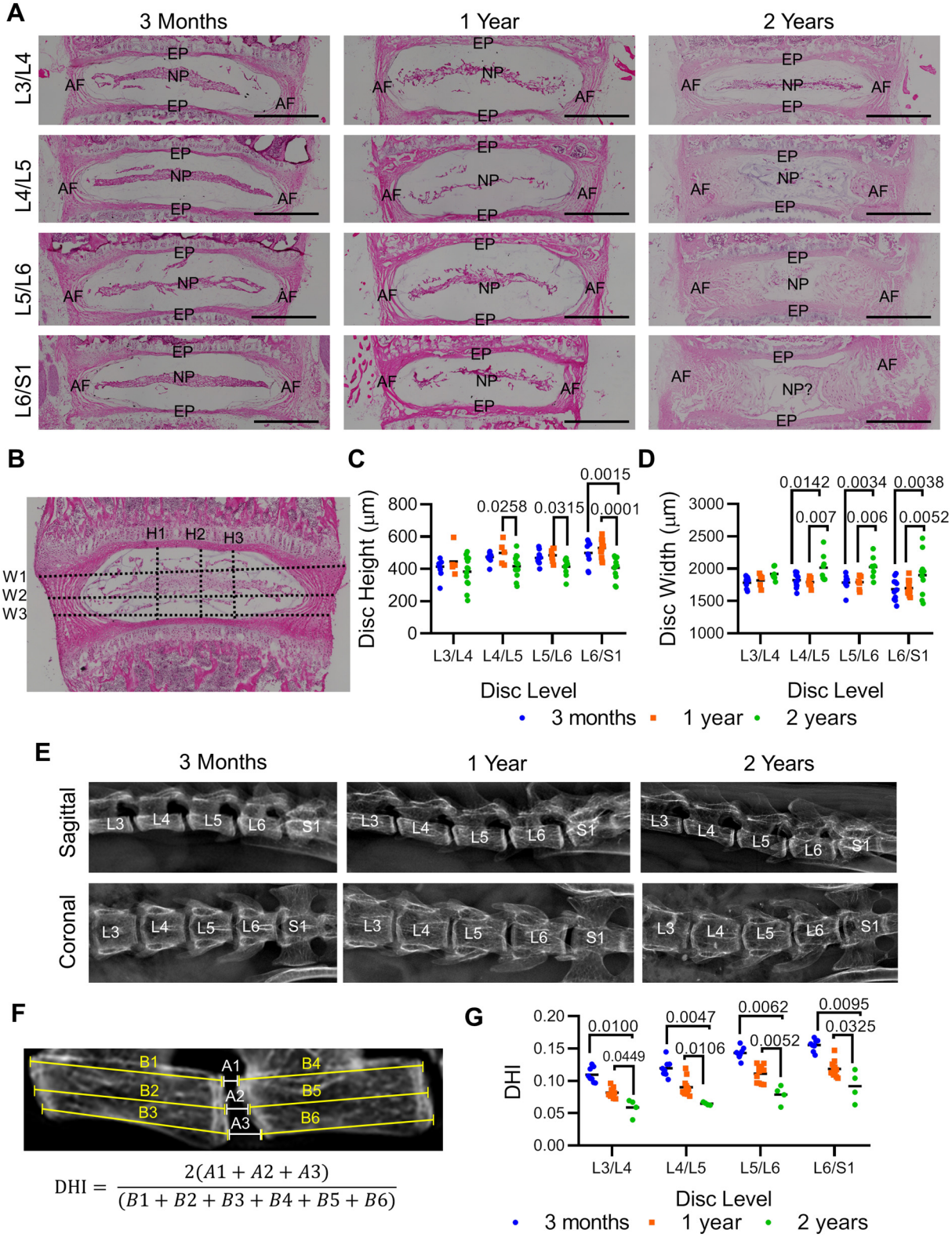

Fig. 1. Morphological changes in the lumbar IVD with age in mice. A) H&E stained mid-coronal sections of L3-S1 IVDs from mice at indicated ages. Scale bar = 500 μm. B) Schema shows how histological images of IVDs were measured to determine IVD height (H1–3, three vertical dotted lines) and width (W1–3, three horizontal dotted lines). C) Quantification of IVD height. Each point represents a unique animal. D) Quantification of IVD width. Three-month-old, n = 7–12 per IVD level (3–5 females per level); one-year-old, n = 6–13 per IVD level (4–8 females per level); two-year-old, n = 10–13 per IVD level (5–7 females per IVD level). E) Radiographs showing the sagittal and coronal view of representative L3-S1 vertebrae at the indicated ages. F) Schema shows measurement of DHI on sagittal radiographs with equation below. G) Quantification of DHI. Each point represents a unique animal. Three-month-old, n = 8 (4 females); one-year-old, n = 12 (5 females); two-year-old, n = 4 (2 females). Horizontal bars represent mean. Dunnett's post-hoc pairwise comparison p-values are above identified groups. AF = annulus fibrosus, EP = endplate, NP = nucleus pulposus.

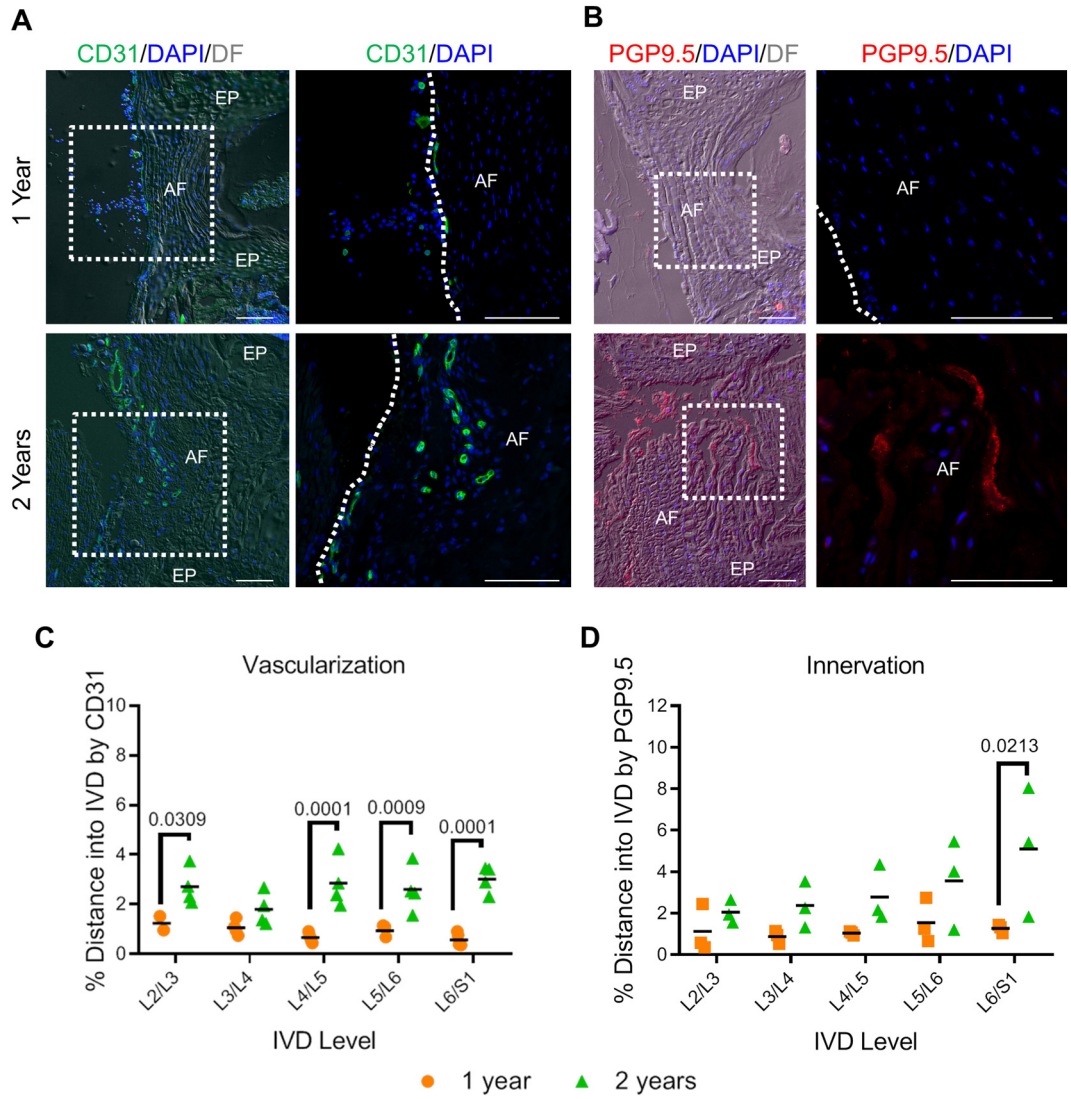

Fig. 2. Vascularization and innervation of the lumbar IVD. A) Representative immunofluorescence for endothelial marker, CD31 shown in green, in the L6/S1 AF of a year-old and two-year-old mouse. B) Representative immunofluorescence for pan-neuronal marker, PGP9.5 shown in red in the L6/S1 AF of year-old and two-year-old mouse. Left panels show low magnification with dark-field (or DIC) to show IVD structure, right panels are high magnification of indicated region. Scale bar = 100 μm. Nuclei are counterstained with DAPI in A and B. C) Quantification of distance into the disc CD31 positive structures appear, normalized by total IVD width. Three-month-old, n = 3–5 per IVD level; one-year-old, n = 2–4 per level; two-year-old n = 4 per IVD level. D) Quantification of distance into the disc PGP9.5 positive structures appear, normalized by total IVD width. N = 3 per age group for all levels. Post-hoc pairwise comparison p-values are above identified groups. AF = annulus fibrosus, EP = endplate, DF = dark-field. (For interpretation of the references to color in this figure legend, the reader is referred to the web version of this article.)

2.3.1. Open field test

The open field test (OFT) [49] consisted of a rectangular arena (50 × 30 cm), with a transparent floor divided into 15 squares (10 × 10 cm), enclosed by continuous, 25 cm high walls made of translucent plastic. The apparatus was placed on a bench top in a well-lit, quiet room. The test was initiated by placing a single mouse in the middle of the arena and letting it move freely for 5 min. The behaviors were scored by the experimenter using a continuous sampling method. The arena was cleaned with Clidox and water after every test. The number of squares crossed was measured as voluntary horizontal mobility and the duration of time spent rearing on hind legs was measured as voluntary standing.

2.3.2. Tail suspension test

The tail suspension assay (TST) [50] was performed as described previously [35,36,38]. In brief, mice were suspended from the underside of a platform 30 cm above the table top using adhesive tape 0.5 cm from the base of the tail. Behaviors were recorded for 3 min while under supervision of the experimenter. The duration of time spent a) reaching towards the ground, b) immobile, c) rearing towards their tail, and d) self-suspended by holding onto the base of the tail, ankle or tape was analyzed over the testing period.

2.3.3. Cold allodynia

Cold allodynia was assessed by measuring nocifensive behaviors after 25 μL of acetone (stored at room temperature) was applied using a pipette to the plantar surface of the hind paw [51,52]. Acetone is a volatile substance that evaporates quickly, cooling the paw. Mice were placed in a 25 × 15 cm translucent plastic cage during the test. Nocifensive behaviors included licking or scratching the affected hind paw and ankle during a two-minute period immediately following acetone application. Both left and right hind paws were tested with a minimum of 15 min between test sessions. The paw order for testing was randomized between animals.

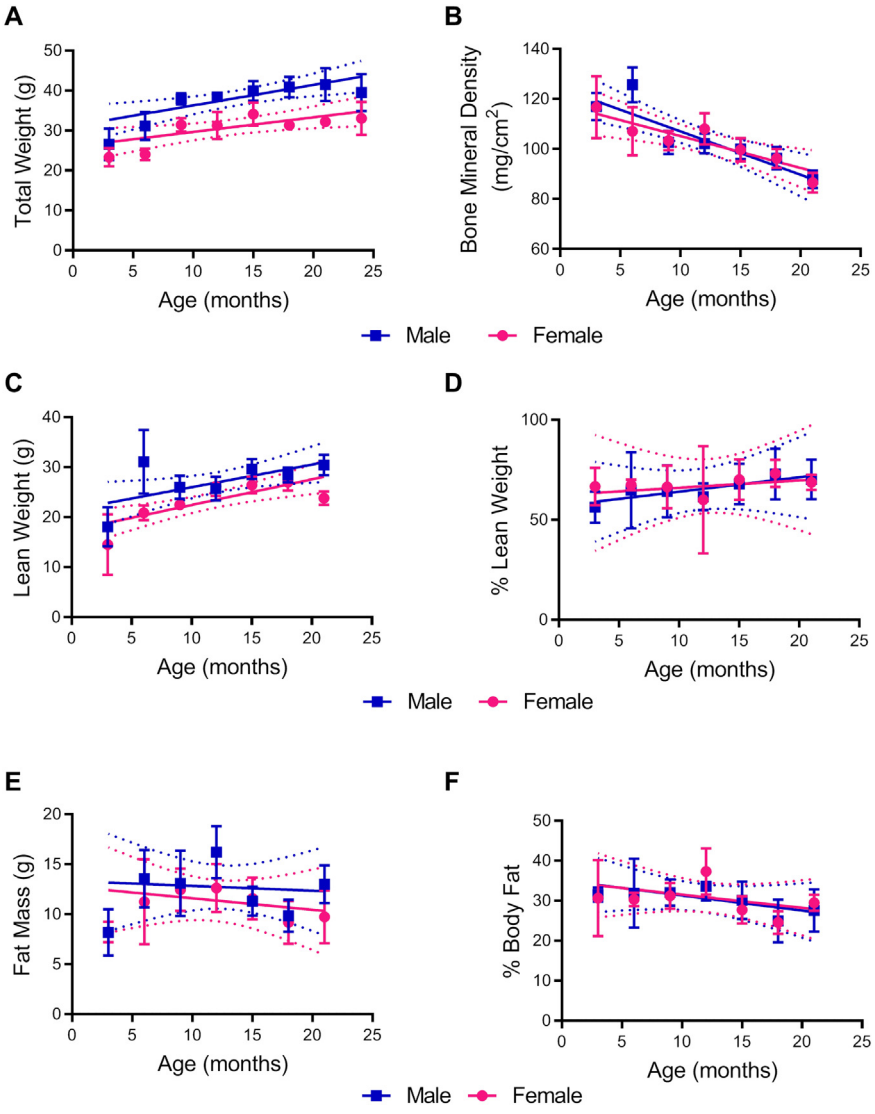

Fig. 3. Body composition in aging mice. Age related changes in A) total weight, B) bone mineral density (BMD), C) lean weight, D) percent lean weight, E) fat mass, and F) percent body fat in male and female mice. Solid lines represent linear regression with 95% confidence intervals in hashed lines. Points represent mean values at indicated age ± S.E.M.

2.3.4. Thermal hyperalgesia

Thermal hyperalgesia was assessed by injecting capsaicin (2.5 µg in 5 µL of 0.25% ethanol, 0.125% Tween-20 in saline) into the dorsal surface of the left hind paw [35]. Capsaicin, the active ingredient in hot chili peppers, acts on TRPV1 receptors which respond to noxious heat and produces a temporary, noxious thermal sensation without damaging the tissue [53]. The duration spent licking or scratching the hind paw during a three-minute period was assessed by continuous sampling method. Only one paw was tested per animal to avoid carry over effects on the second hind paw.

2.4. Tissue collection

Vertebrae from the cervical to caudal levels were dissected from mice at identified time points and placed in ice-cold 1× phosphate buffered saline (PBS). A laminectomy was performed as previously described [54] to expose the spinal cord and DRGs. L4 and L5 DRGs were extracted and fixed in buffered 4% paraformaldehyde (PFA) in PBS for 4 h at 4 °C and cryoprotected overnight in 30% sucrose at 4 °C. DRGs were molded in Tissue-Tek® Optimal Cutting Temperature (O.C.T.) compound and stored in −80 °C until sectioned. Following DRG extraction, the lumbar vertebrae from L2 to S1 was fixed in buffered 4% PFA in PBS for 4 h at 4 °C. Vertebrae were decalcified in 0.5 M ethylenediamine tetracacetic acid (EDTA), pH 7.4 for 7–9 days at 4 °C with twice daily solution changes. Vertebrae were molded in O.C.T. compound and store in −80 °C until cryosectioned.

2.5. Histology

Vertebral cryosections from the L2 to S1 level were collected at 8 µm thickness in the coronal or transverse plane using a Leica cryostat. Sections were stored at −20 °C for later use. Histology of the vertebrae in the coronal plane was analyzed by staining with hematoxylin and eosin (H&E) using 8–13 animals per age group, both male and female. Sections were photographed using a Nikon Eclipse microscope. IVD height was measured using NIS-Elements Advanced Research Analysis software, selecting mid coronal sections and measuring the NP space height (excluding the endplate) in three locations along the straight region of the IVD and averaged. IVD width was measured similarly by measuring three locations along the entire width of the IVD, from the outer left AF to outer right AF, and taking the average of the three.

Table 2
General linear model results of behavioral assays.

Assay	IV	DV	F	Sig.	Partial η^2
Open field test (OFT)	Corrected model	OFT_mobility	4.850	**0.0003**	0.097
		OFT_standing	10.824	**0.000**	0.194
	Age	OFT_mobility	2.627	0.107	0.019
		OFT_standing	23.255	**0.000**	0.147
	Weight	OFT_mobility	0.090	0.765	0.001
		OFT_standing	0.020	0.887	0.00
	Sex	OFT_mobility	11.231	**0.001**	0.077
		OFT_standing	70107	**0.009**	0.050
Tail suspension test (TST)	Corrected model	TST_reach	6.923	**0.000**	0.140
		TST_immobile	3.302	**0.023**	0.072
		TST_rear	3.454	**0.019**	0.075
		TST_SS	1.988	0.119	0.045
	Age	TST_reach	13.387	**0.000**	0.095
		TST_immobile	3.461	0.065	0.026
		TST_rear	9.999	**0.002**	0.072
		TST_SS	2.857	0.093	0.022
	Weight	TST_reach	0.939	0.334	0.007
		TST_immobile	2.569	0.111	0.020
		TST_rear	1.774	0.185	0.014
		TST_SS	0.215	0.644	0.002
	Sex	TST_reach	2.892	0.091	0.022
		TST_immobile	0.608	0.437	0.022
		TST_rear	0.435	0.551	0.005
		TST_SS	2.393	0.124	0.003
Cold allodynia and thermal hyperalgesia	Corrected model	Acetone	16.347	**0.000**	0.209
		Capsaicin	1.171	0.322	0.019
	Age	Acetone	47.694	**0.000**	0.204
		Capsaicin	1.462	0.228	0.008
	Weight	Acetone	14.890	**0.000**	0.074
		Capsaicin	2.744	0.099	0.015
	Sex	Acetone	1.068	0.303	0.006
		Capsaicin	1.852	0.175	0.010

IV = independent variable, DV = dependent variable, OFT_mobility = number of squares crossed in the OFT, OFT_standing = amount of time spent standing in the OFT, TST_reach = time spent reaching in the TST, TST_immoline = time spent immobile in the TST, TST_rear = time spent rearing in the TST, TST_SS = time spent self-suspended in the TST, Acetone = cold allodynia score, capsaicin = thermal hyperalgesia score. Bold values indicate $p < 0.05$.

2.6. Immunofluorescence

Immunostaining was carried out on 8 µm thick cryosections of fixed lumbar DRGs and IVDs. The sections were permeabilized using PBS containing 0.25–0.5% Triton-X 100 for 10 min, blocked in blocking buffer (10% normal donkey serum, 4% IgG-free bovine albumin in PBS containing 0.1% Triton-X100 (PBST)) for 1 h at room temperature, treated with primary antibody (1:100 Guinea Pig anti-NaV1.8, AGP-029, Alomone labs, Jerusalem; 1:100 rabbit anti-NaV1.9, ASC-017, Alomone labs, Jerusalem; 1:50 goat anti-CD31/PECAM-1, AF3628, R&D systems, USA; 1:50 rabbit anti-PGP9.5/UCH-L1, NB110-58874, Novus Biologicals, USA) overnight at 4 °C in a humidified chamber, washed in PBST 3 × 7 min, treated with appropriate secondary antibody (1:200 donkey anti-guinea pig conjugated to Alexa Fluor®594 706-585-148; 1:200 donkey anti-rabbit conjugated to Alexa Fluor® 647, 711-605-152; 1:200 donkey anti-goat conjugated to Alexa Fluor® 488, 705-545-147, all from Jackson Immuno Research Laboratories) in blocking buffer for 1 h at room temperature, washed in PBS 3 × 7 min, and counterstained with 1:5000 DAPI to stain the cell nuclei. The slides were mounted in PBS containing 50% glycerol and 25 µg/mL of anti-quenching agent DABCO (D27802, Sigma). Images were captured using a Nikon Eclipse microscope under the same conditions to maintain image homogeneity. A negative control accompanied each immunostaining session wherein all the steps were followed but the primary antibody was omitted.

Innervation and vascularization analysis of the IVDs was quantified using the measure tool in NIS-Elements Advanced Research microscopy imaging software. The distance between the PGP9.5 or CD31 positive bodies and the outer AF was divided by the total width of the IVD. Mean fluorescent intensity (MFI) analyses of DRGs were carried out using the region of interest tool in the NIS-Elements Advanced Research microscopy imaging software. Measurements were performed by outlining 50 cells for each DRG section by a researcher blind to the age condition. Cell selection was performed by choosing one cell and measuring all nearest neighbors until a cell count of 50 has been reached. Cells of varying sizes were captured for all DRGs and cell size distribution did not differ significantly between samples, indicative of unbiased sampling (Supplemental Fig. 2).

2.7. Statistical analysis

All statistics were carried out using IBM SPSS statistics 24 software. A two-way mixed factor ANOVA was used to compare IVD height, width, innervation and vascularization across ages and IVD level, with post-hoc comparisons made using Dunnett's test. Sample sizes for morphometric analysis on histological samples were between 8 and 13 mice per age group and IVD level. Sample size for disc height index measures on radiographic samples were between 5 and 8 mice per age group. Sample size for vascularization was between three to four mice per age group, and three mice per group were used for innervation analysis. Body composition measures and their relationship to age and sex were analyzed by linear regression. All behavioral tests were analyzed using a general linear model with sex as a factor and age and weight used as covariates. Post-hoc analysis on general linear model was performed using Bonferroni's test for multiple comparisons. Immunofluorescence data was analyzed by comparing the median value of the MFI in each animal's L4 and L5 DRG and performing a two-way mixed factor ANOVA with the repeated measured being DRG level and the between factor being age group. Dunnett's test for post-hoc comparison was used to evaluate simple main effects of each DRG level.

3. Results

3.1. Shortening and bulging of the lumbar IVD with age in mice

With age, the human IVD undergoes pathological changes, including bulging, collapse, herniation and tears, which are more likely than not to be symptomatic [55]. In particular, patients with LBP present with shorter lumbar IVDs than those without [56]. This is particularly common in the lumbosacral level L5/S1, followed by L4/L5 then L3/L4 [56]. The vulnerability of these levels in humans may be in part due to the axial loading forces imposed by our bipedalism. Despite their quadrupedal stance, however, the lumbar IVDs in mice have comparable mechanical properties [57] and similar geometry [58] to the human disc. It has also been established that mouse cervical IVDs become progressively more degenerated with age [30]. To assess similar age-related changes in the lumbar IVD (of which there are typically 6) with physiological age, H&E stained mid-coronal sections of the lumbar IVD were analyzed in three-month (young adult), one-year (mid-aged adult), and two-year-old (old-aged adult) male and female mice (Fig. 1A, n = 8–13 per age group). Young mice have a uniform lumbar IVD structure; the NP is spread and reticular and the AF is tightly organized in distinct layers. By one year, the lumbar IVD remains structurally intact, though NP spread is less diffuse and the AF layers are more loosely associated as previously shown [59]. Two-year-old mouse lumbar IVDs have diverse phenotypes and hypo-cellularity, a feature correlated with aging in human IVDs [60] and previous reports of cervical [30] and lumbar [59,61] IVDs in aging mice. Notably, few cells are seen in the NP space and the inner layers of the AF appear disorganized and invade the NP space (Fig. 1A, Supplemental Fig. 1). The IVD height and width were measured on the H&E stained mid-coronal sections (illustrated in Fig. 1B). Quantification of IVD heights by two-way ANOVA revealed that two-year-old mice regardless of sex have shorter ($p < 0.0001$) IVDs than both three-month and year-old

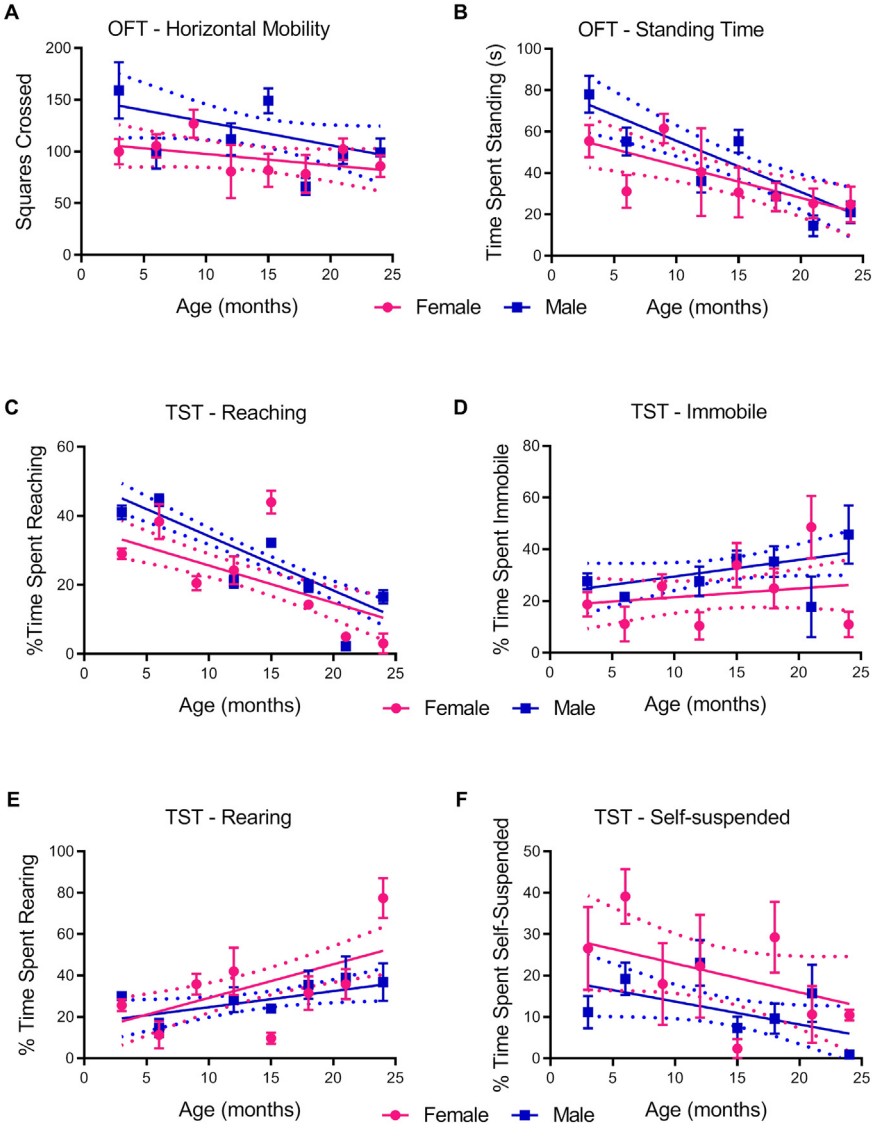

Fig. 4. Axial stretching in aging mice. A) Age-related changes in the number of squares crossed (horizontal mobility) and B) time spent standing on hind quarters in an open field test (OFT). s = seconds. Percent time spent in C) reaching, D) immobile, E) rearing, and F) self-suspended positions by male and female mice in the tail suspension test (TST). Data points represent means ± S.E.M. Solid lines represents linear trend of female and male mice, hashed lines represent 95% confidence interval of regression.

mice (Fig. 1C), and the most caudal levels, L4 to S1 were most affected. A two-way ANOVA also found that two-year-old IVDs regardless of sex are significantly wider ($p < 0.0001$) than both three-month and year-old IVDs. Again, the caudal lumbar IVDs were most affected in advanced age (Fig. 1D). No differences in height or width were observed between young adult and middle-aged mice, suggesting these changes begin to occur after one year of age.

To avoid measurement bias due to sectioning and histological artifacts, radiographs of the lumbar spine of three-month, one-year and two-year-old mice was captured in coronal and sagittal plane (Fig. 1E) to determine the age-related changes in disc height index (DHI [48], illustrated in Fig. 1F). Compared to both three-month-old and year-old mouse lumbar IVDs, two-year-old lumbar IVDs show a significant reduction in DHI (Fig. 1G, n = 5–8 per age group). Taken together, these data suggest that despite their quadrupedal lifestyle, aged mice do develop degenerated IVDs resulting in the shortening and bulging of the caudal lumbar IVDs.

3.2. Increased vascularization and innervation of IVDs with age in mouse

The structural changes that characterize IVD degeneration in humans, in particular the loss of collagen-rich and organized AF, allows for vascular bodies and nerves to enter further into the normally avascular, anneural IVD [62,63]. To assess whether similar changes occur in the degenerated discs with age in mice, immunofluorescence for endothelial cell marker, CD31 [64] (or PECAM-1), and pan-neuronal marker, PGP9.5 (or UCHL1) [65,66], was used to detect vascular and neural structures on the mid-coronal sections of the lumbar IVD. The distance at which either CD31 and PGP9.5 positive structures appears into the IVD from the outer edge of the AF as a percentage of the total IVD width was used to quantify innervation and vascularization depth. In the healthy year old IVDs, CD31 positive structures are detected along the outer surface of the AF (Fig. 2A). In two-year-old mice, these structures are often seen deeper into the outer AF layers (Fig. 2A). Similarly, PGP9.5 positive structures are largely absent in year-old IVDs, but are found in the outer layers of the AF of degenerated aged IVDs of two-year-old mouse (Fig. 2B). Analysis by two-way ANOVA reveals that vascular structures appear further into the lumbar IVDs in two-year old

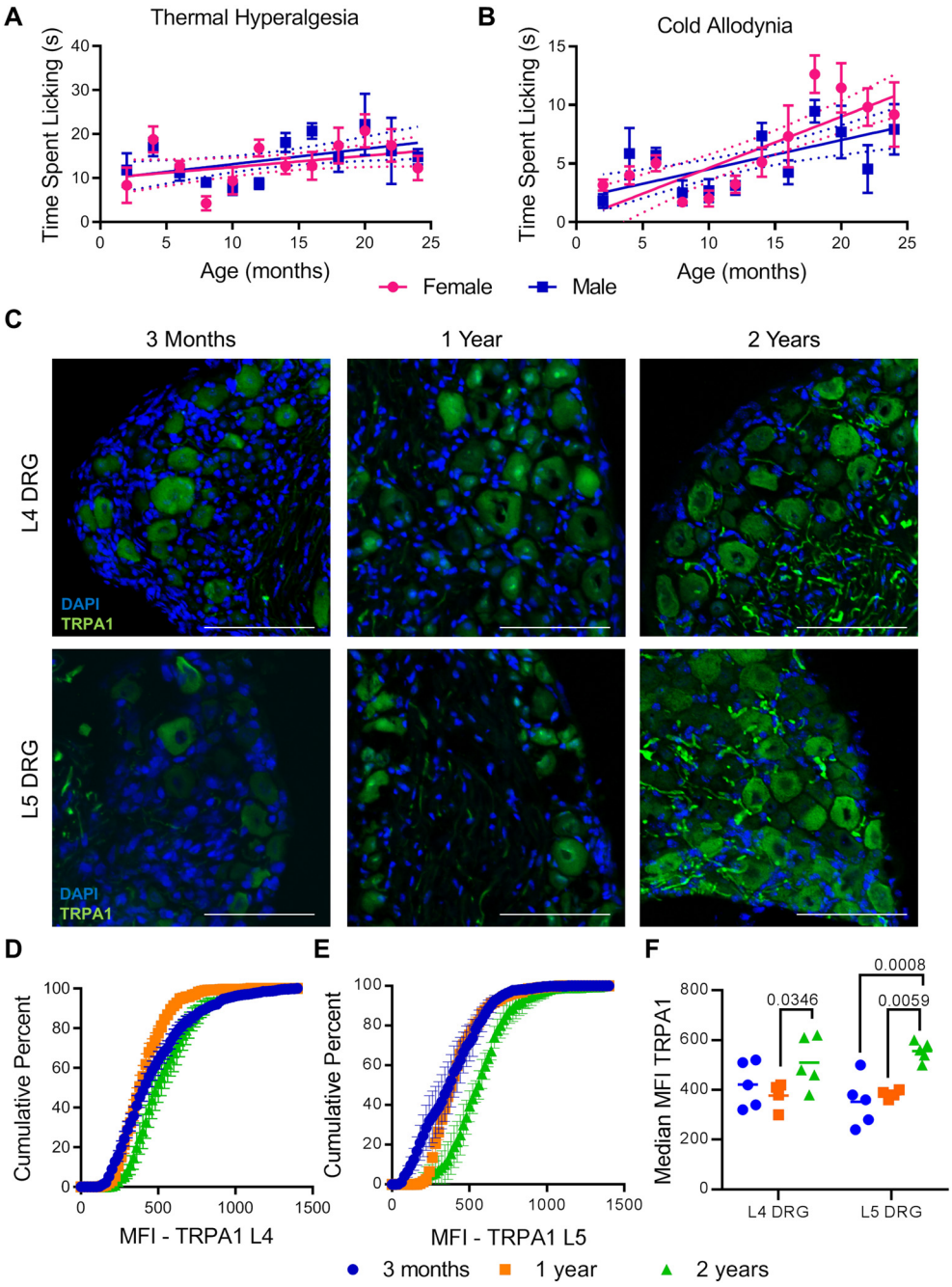

Fig. 5. Radiating cold allodynia and thermal hyperalgesia with age in mice. A) Thermal hyperalgesia in male and female mice from 2 to 24 months of age. The amount of time spent licking the left hind paw in response to a subcutaneous capsaicin injection into the left hind paw in mice of varying ages. B) Cold allodynia in male and female mice from 2 to 24 months of age. The amount of time spent licking the hind paws in response to a dermal application of acetone. s = seconds. Data points are means ± S.E.M. Solid lines represents linear trend, hashed lines represent 95% confidence interval of regression lines. C) Representative immunofluorescence of TRPA1 in L4 and L5 DRGs in mice at indicated ages. Scale bars = 100 μm. D–E) Cumulative frequency distribution of the TRPA1 mean fluorescent intensity (MFI) of L4 (D) and L5 (E) DRGs. Points represent mean of 5 mouse distributions ± S.E.M. F) median MFI of TRPA1 L4 and L5 DRGs of each animal from D and E. Dunnett's post-hoc p-value above indicated comparisons.

mice than year old mice (Fig. 2C, $p < 0.0001$, n = 3–4), and PGP9.5 positive structures appear deeper only in the lumbosacral IVD (Fig. 2D, $p = 0.0187$, n = 3 per group). These results provide evidence of increased vascularization of the lumbar IVDs, but limited innervation in physiologically aging mice. Vascularization and innervation in human IVDs is associated with painful degeneration [62,63]; it remains to be seen whether these features correlate in mice.

3.3. Weight gain and loss of BMD in aging mice

With advanced age, changes in body composition are regularly reported in human populations. These changes include a loss of BMD with age, increased percent body fat with age, and an increase in lean muscle mass until mid-age, followed by a decline into old-age [67]. These factors provide useful context for understanding degenerative changes – including disc degenerative changes and LBP – that accompany aging. To assess whether aging in mice was associated with similar changes in body composition, DEXA scans were performed on male and female mice between three to 21 months of age. Total weight significantly increases over the course of the mouse lifespan in both females ($F(1,133) = 6.069$, $p = 0.0150$) and males ($F(1,159) = 9.216$, $p = 0.0028$), with males weighing on average 5 g more than females (Fig. 3A). Similar to humans, BMD decreases with age in both female ($F(1, 42) = 14.94$, $p = 0.0004$) and male ($F(1, 43) = 9.976$, $p = 0.0029$) mice (Fig. 3B). Interestingly, lean weight continues to increase in both female ($F(1, 42) = 12.24$, $p = 0.0011$) and male ($F(1, 43) = 5.306$, $p = 0.0262$) mice with age (Fig. 3C); however, this linear relationship with age is lost when controlling for total body weight (Fig. 3D). Thus, lean weight increases proportionately to total weight with age in mice. Lastly, unlike in humans, neither fat mass nor percent fat mass was linearly associated with aging in mice (Fig. 3E–F). Taken together these data indicate that body composition in terms of percent body fat and

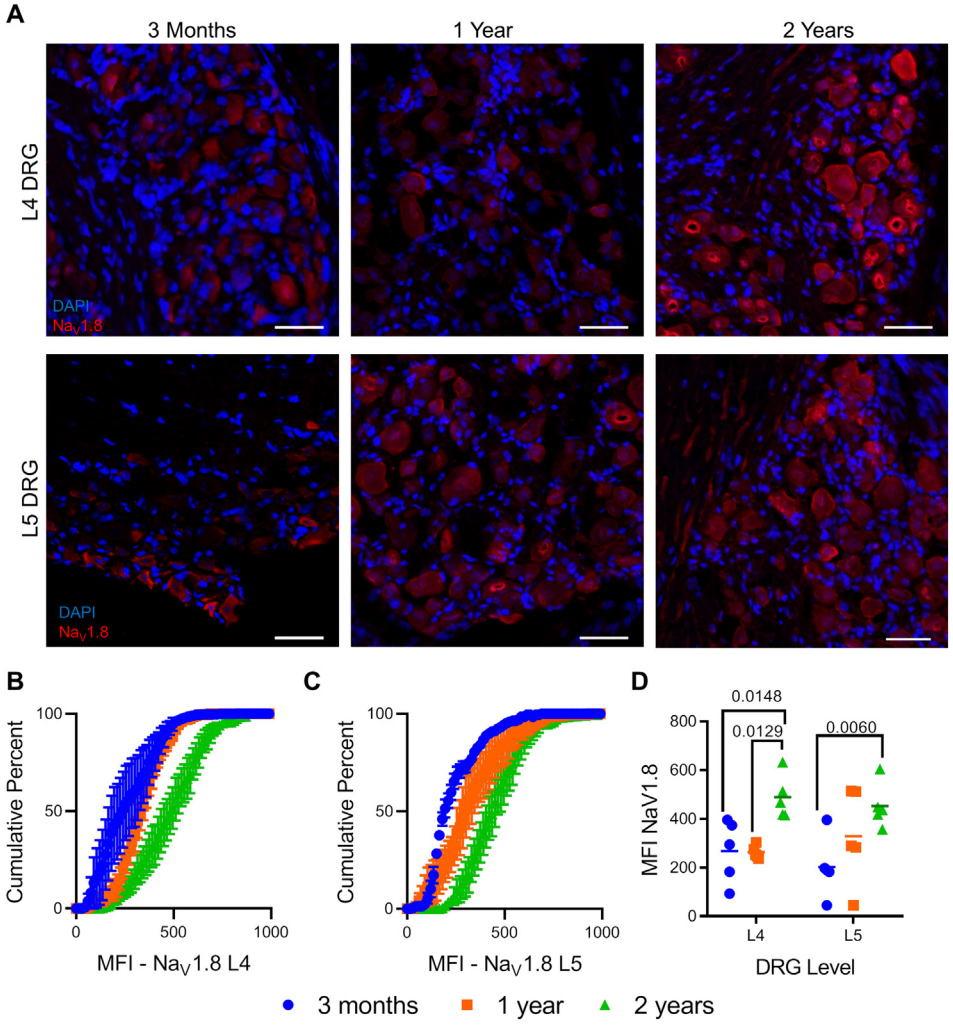

Fig. 6. Changes of $Na_V1.8$ in L4 and L5 DRGs with age in mice. A) Representative immunofluorescence of $Na_V1.8$ in the L4 and L5 DRGs at indicated ages. Scale bar = 50 μm B–C) Cumulative frequency distribution of the $Na_V1.8$ mean fluorescent intensity (MFI) of L4 (B) and L5 (C) DRGs. Points represent mean of 5 mouse distributions ± S.E.M. D) Median MFI of $Na_V1.8$ L4 and L5 DRGs of each animal from B and C. Dunnett's post-hoc p-value above indicated comparisons.

percent lean mass is unchanged in aging mice, indicating that degenerative changes are not driven by these measures. However, increase in overall weight and loss of BMD with aging are both important features to consider in aging mice.

3.4. Effects on standing, stretching and mobility with age in mice

There is no single behavioral assay that can accurately capture the presence of LBP in mice. Instead, we rely on multiple assays to assess behaviors that correlate with impairments seen in humans with LBP. One of the manifestations of LBP in patients is its negative impact on functional movements [45,46]. For instance, patients with LBP are more likely to modify movements to avoid lower lumbar motion than those without LBP [47]. To assess the impact of age on similar functions in mice, 222 mice of both sexes, ranging from two to 24 months of age were assayed for behavioral correlates of back pain (Table 1). As mouse weight significantly correlated with age (Fig. 3A) and may impact these assays independently of age, weight was also added as a dependent variable in all behavioral statistical models. A modified open field test (OFT) was used to measure both mobility and voluntary standing [68]. Mobility was measured as the number of squares (10 cm × 10 cm) crossed on all four limbs in an open arena and assesses voluntary horizontal movement. Voluntary standing was the amount of time (in seconds) the mice spent standing on hind limbs while exploring the arena, a position which produces axial stretching, requires trunk stability and lower body strength. A general linear model was run to assess the relationship between age, weight, sex, mobility and voluntary standing in an open field (Table 2). The model revealed that as mice age they continue to walk unimpaired in the arena (Fig. 4A), but spend less time standing up while exploring (Fig. 4B). Thus, aged mice remain mobile and explore novel environments, but opt to remain on all four limbs while exploring. The reluctance to stand is not likely due to a loss of strength or muscle wasting as muscle mass increases with age and remains proportional to total body weight (Fig. 3C and D). Instead it may be associated with an increase in discomfort when standing either due to LBP or other musculoskeletal discomfort; alternatively, it may represent a loss of energy or motivation with aging.

To more directly assess the contribution of stretch avoidance during aging we employed the tail suspension test (TST) which has been modified and validated for measuring axial back pain in the mouse [35,36,38]. This assay forces the mouse into a position of axial stretching by suspending the animal by its tail above a surface, prompting escape responses. The mouse may partition its time into positions that exacerbate the axial stretching by reaching towards the ground and hanging immobile, or positions that avoid stretching by rearing up towards the source of suspension into a hunched position or self-suspending by holding onto their own foot or tail for support. Critically, unlike standing in the OFT, reaching and rearing behaviors

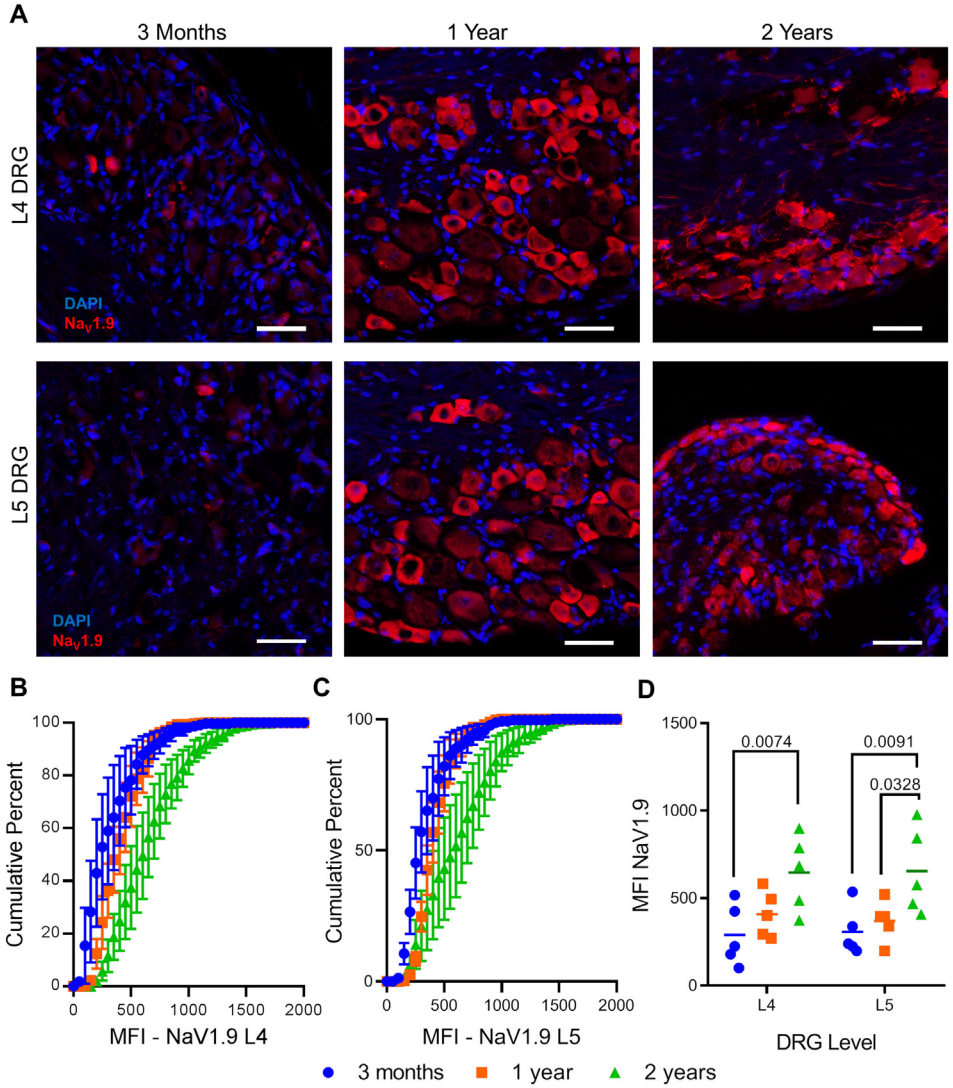

Fig. 7. Changes of $Na_V1.9$ in L4 and L5 DRGs with age in mice. A) Representative immunofluorescence of $Na_V1.9$ in the L4 and L5 DRGs at indicated ages. Scale bar = 50 μm. B–C) Cumulative frequency distribution of the $Na_V1.9$ mean fluorescent intensity (MFI) of L4 (B) and L5 (C) DRGs. Points represent mean of 5 mouse distributions ± S.E.M. D) Median MFI of $Na_V1.9$ L4 and L5 DRGs of each animal from B and C. Dunnett's post-hoc p-value above indicated comparisons.

do not put pressure on the knee joints which are likely also impacted by age. The general linear model (Table 2, Fig. 4C–F) reveals that the time spent reaching (Fig. 4C) and the time spent rearing (Fig. 4E) are both predicted by age. Importantly, with age, mice spend less time reaching towards the ground and more time rearing towards the platform. Interestingly, there was no significant effect of age on time spent immobile (Fig. 4D), which historically has been used as a measure of despair [50], suggesting older mice do not simply get tired or have greater despair than young mice in this task. Instead, older mice will perform a rearing action to avoid axial stretching in the TST, which is consistent with stretching along the axis producing discomfort. Lastly, time spent in a self-supported position is not affected by age, sex, or weight in mice (Table 2, Fig. 4F). Taken together with the OFT, these results suggest that mice will both passively and actively avoid positions that exacerbate axial stretching.

3.5. Cold allodynia and thermal hyperalgesia with age in mice

Radiating pain is a feature observed more commonly in the elderly with LBP than younger patients [69], and has been attributed to compression or damage to the sciatic nerve [70]. While radiating pain in humans is generally described verbally, animal models rely on showing hypersensitivity to stimuli as a proxy for pain. To test for the presence of radiating pain with age in mice, thermal hyperalgesia [35] using capsaicin, and cold allodynia [52] using acetone in the hind paws, a region innervated by the sciatic nerve, was assessed. Capsaicin is the active ingredient in hot peppers and is a ligand for the heat-activated channel, TRPV1 [71]. When injected into the left hind paw, mice respond by licking the area (Fig. 5A). However, this behavior is not associated with age, sex, or weight (Table 2). In contrast, response to acetone, which cools the skin it touches, is associated with age in the general linear model (Table 2, Fig. 5B). Results revealed that both age and weight significantly ($p < 0.0001$) predict cold allodynia responses; mice that were older and mice that weigh less are more likely to respond to acetone.

Increase in cold sensitivity with age in mice prompted us to measure whether there is a respective increase in the levels of noxious cold channel, TRPA1 [72], in the L4 and L5 DRGs using immunofluorescence analysis. L4 and L5 DRGs account for 95% of the cells that make up the sciatic nerve [73] which innervates the hind paw. To determine relative levels of TRPA1, the mean fluorescent intensity (MFI) of 150 individual neurons within the L4 and L5 DRGs of each mouse was measured and the distribution plotted, revealing a rightward shift in aged mice (Fig. 5C - E). Taking the median MFI value of L4 and L5 DRGs and using

a two-way ANOVA revealed that two-year-old mice showed a greater accumulation of TRPA1 compared to year-old mice in both the L4 and L5 DRGs, but was only greater than three-month-old mice in L5 DRGs (Fig. 5F). These results are consistent with the observed increased reactivity to acetone in aged mice validating the increased sensitivity to cold allodynia with age in mice.

3.6. Accumulation of TTX-resistant sodium channels in L4 and L5 DRG of aged mice

The avoidance of stretching and increased radiating cold allodynia may also be due to increased sensitivity of the sensory nerves. To test for signs of sensitization in the peripheral pain pathway, the presence of sodium channels $Na_V1.8$ and $Na_V1.9$ in the L4 and L5 DRGs was measured by immunofluorescence (Figs. 6 and 7). $Na_v1.8$ [74] and 1.9 [75] are expressed in small nociceptive DRGs and contribute to nociceptive signaling by allowing for sustained repetitive firing in these cells. To capture changes in the accumulation of $Na_V1.8$, the MFI of individual neurons within the L4 and L5 DRGs was measured and the distribution plotted (Fig. 6A–C). Taking the median MFI of each DRG and running a two-way ANOVA revealed that two-year-old mice have a greater $Na_V1.8$ MFI in L4 and L5 DRGs compared to three-month old, and a greater $Na_V1.8$ MFI in the L4 DRG compared to one-year old (Fig. 6D). Similarly, the accumulation of $Na_V1.9$ in the L4 and L5 DRGs was analyzed as discussed above (Fig. 7A–C). A two-way ANOVA also revealed that two-year-old mice have greater $Na_V1.9$ MFI in the L4 and L5 DRGs than three-month-old and greater MFI than one-year-old L5 DRGs (Fig. 7D). These results confirm that there are changes in the nociceptive signaling pathway in the L4/L5 DRGs consistent with reduced pain thresholds in aged mice.

4. Discussion

LBP is a feature of aging which begins to emerge by 20 years, with increasing rates reported until 60–65 years [76]. Because of the multitude of risk factors that lead to LBP, isolating the effects of age independently from environmental, hereditary and lifestyle factors is complicated in human populations. Pre-clinical studies often rely on mouse models to delineate features of disc degeneration as it relates to human populations. A major concern in these studies is how well the quadrupedal posture serves as a proxy for human intervertebral disc physiology. Here we assess the progression of IVD degeneration with behavioral and molecular correlates of pain in a controlled and physiologically aging mouse model system. Despite the differences in posture, we show that mice lumbar IVDs do undergo progressive degenerative changes with advanced age. Furthermore, we show mobility and cold sensitivity changes as a function of physiological aging in mice.

A commonly cited risk factor for LBP in the elderly is IVD degeneration. In the aging IVD, structural defects such as neovascularization, tears, and cell death become more common [77]. These defects are painful in part due to the rise in pro-inflammatory molecules secreted in aging and degenerating discs [78,79]. Historically, much attention has been given to TNF-α and IL-1β, whose expression is elevated in degenerated IVDs [80–82]. Both TNF-α and IL-1β expression in the disc has been associated with sensory nerve ingrowth [83,84], a feature characteristic of painful discs in patients [63,85,86] and observed in our two-year-old mice. In human IVD tissue, IL-1β expression is also strongly correlated with expression of vascular endothelial growth factor, VEGF, the presence of which is predictive of CD31 expression in the disc [84]. Further, expression of TNF-α and its receptor, TNFR1, in the IVD is positively correlated with scores on the visual analog scale for pain in patients six months following a discectomy, suggesting inflammation contributes to LBP chronicity [86]. Pro-inflammatory mediators are also expressed at elevated levels in aged mouse IVDs. In addition to IL-1β, 28-month-old mice have increased expression of NF-κB, iNOS, and IL-6 as well as collagenases, MMP-1b and MMP-3 [87]. This transition to a detrimental pro-inflammatory state in aging mouse IVDs tracks well with the structural and histological changes to the IVDs reported here and by others [30,34], and may contribute to the development of pain behaviors in aged mice.

Longitudinal studies in elderly adults point to an association between LBP and loss of IVD height [88,89]. In our study, loss of IVD height, reduced DHI and increased IVD widening was only apparent by the very late stages of life in mice, and, similar to humans [56], the caudal lumbar IVDs were the most affected by age. By two years of age we also observe histological changes in the lumbar IVDs, consistent with previous reports in aged mice [61]. Importantly, disc height and width was maintained between young adulthood to middle-age in mice, suggesting degeneration has a later onset in mice than in humans. Thus, despite the absence of injury, lifestyle-related risk factors, and bipedalism that contribute to degeneration in humans, IVD degeneration spontaneously occurs in aged mice.

Mouse models of IVD degeneration using mechanical injury or genetic mutation confirm that disc degeneration produces a range of painful behavioral phenotypes [17,21,31,35,37–39]. While mechanical allodynia is often reported in the short-term injury-induced models of IVD degeneration [17,20], the same is not observed in genetic models where disc degeneration develops slowly [37,38], nor in aged control mice [35]. More compelling are measures capturing mobility changes and impairment, as these features are clinically relevant to features of LBP in older adults, with 15–46% of individuals over the age of 65 reporting physical limitations due to LBP [90]. We found that mice are increasingly unlikely to take bipedal positions as they get older and will take action to mitigate axial stretching when forced. SPARC-null mice, which display early-onset advanced IVD degeneration, likewise avoid positions that exacerbate axial stretching [35]; however, changes in tail suspension behavior due to vestibular balance or proprioception effects in aging mice cannot be discounted. Voluntary standing behavior places additional force on the lumbar IVDs, as evidenced by the advanced IVD degeneration observed in bipedal mouse models [91], and may discourage mice with painful disc degeneration from such positions. Although we see an increase in age-related disc degeneration and pain in our study, we cannot identify the underlying causes for the change in behaviors as aged mice are physiological and metabolically different from young. One contributing factor to reduced standing time may be lower BMD in older mice, leading to bone frailty. Another is greater levels of circulating pro-inflammatory mediators which is characteristic in aged human populations [92,93], leading to muscular and joint pains. It is unlikely, however, to be due to loss of muscle mass as it is not adversely affected by aging in these mice.

While we did not observe age-related impairments in walking mobility, the assays used here do not capture changes in walking patterns in older mice. Experiments using gait analysis tools report shorter stride length and slower stepping speed following disc injury [21]. Aged mice (two years and older) also have slower gait speed [94,95], shorter travel distances [95,96] and greater standing time [97], which are features also observed in patients with radiculopathy [46]. Thus, gait changes as well as standing and stretching behaviors may be biologically relevant measures for assessing impairment and discomfort in mice.

Because of its relationship to the health of the spine, it is not surprising that the prevalence of radiating LBP is greatest in older patients [98], with cold sensitivity in the regions corresponding to the L4, L5 and S1 dermatomes being reported [99]. Cold sensitivity is also reported in both injury [20] and genetic models [34,35,37] of disc degeneration. Similarly, we found that sensitivity to cold was associated with aging in mice, along with an increase in the TRPA1 channel in DRGs. Unlike pain models which employ unilateral injuries, our study cannot detect reliable left-right differences in allodynia as both sides are equally likely to be affected during aging. Interestingly, although burning pain is a common feature of painful radiculopathy [100],

reports of thermal sensitivity are inconsistent [101,102]. In our aging mice, thermal hyperalgesia was not linearly associated with aging nor any other measure. Others have reported a similar absence of thermal hyperalgesia in LBP models [35]. The absence of thermal sensitivity may be related to a loss of TRPV1 expression reported as early as one year in mouse spinal cords [103].

The presence of pain-related behaviors in aged mice invites the question regarding changes in the somatosensory system in these animals. We observed a marked increase in $Na_V1.8$ and $Na_V1.9$ immunofluorescence intensity in the lumbar DRGs of two-year-old mice, but not in one-year-old mice. As with the changes in the IVD morphology, this phenotype does not appear in middle-age, but rather at the very late stages of life which may be due to the lifestyle factors of laboratory mice. Accumulation of these receptors in DRG cells has been previously reported to occur in models of neuropathic pain as a result of post-translational modification [104], and in models of LBP in mice [26]. It has also been found that sodium channels are phosphorylated following injury, allowing for greater current density and increased nociceptive signaling [104,105]. Future studies will benefit from identifying whether similar changes are occurring as a result of age-related painful degeneration.

The findings of this study describe degenerative and painful features arising in physiologically aging, laboratory-raised mice. As a result, the time course of all the phenotypes observed is reflective of a largely sedentary lifestyle with little chance of injury or strain, possibly delaying onset of degenerative aging phenotypes. While degenerative features appear in the IVD, aging and degeneration of the whole body is occurring simultaneously and a confluence of factors is likely contributing to the behavioral changes described. These changes include attenuated standing and stretching behaviors and radiating cold allodynia, as well as accumulation of excitatory sodium channels in the lumbar DRGs. These results provide important groundwork for characterizing models that attempt to recapitulate features of aging specific to the IVD in a mouse model system.

Acknowledgements

Research reported in this publication was supported by the National Institute of Arthritis and Musculoskeletal and Skin Diseases of the National Institutes of Health under Award Number R01AR065530 awarded to C.L.D. The content is solely the responsibility of the authors and does not necessarily represent the official views of the National Institutes of Health. The research award from Gerstner Family Foundation and S & L Marx foundation made to C.L.D. also supported the research.

Author contributions

C.L.D. conceived and designed the study, and supervised the project. K.V. and C.L.D. wrote the manuscript and prepared the figures. K.V. and S.M. collected data. K.V. performed the data analysis. R.P. R.B. and P.P. provided technical assistance. C.L.D., K.V. and T.J.A. interpreted the data. All authors reviewed the manuscript and gave their final approval.

Competing interests

The authors declare no competing interests.

Appendix A. Supplementary data

Supplementary data to this article can be found online at https://doi.org/10.1016/j.bone.2019.03.037.

References

[1] E.M. Crimmins, H. Beltrán-Sánchez, Mortality and morbidity trends: is there compression of morbidity? J. Gerontol. Ser. B Psychol. Sci. Soc. Sci. 66 B (2011) 75–86.
[2] Hurwitz, E. L., Randhawa, K., Yu, H., Côté, P. & Haldeman, S. The Global Spine Care Initiative: a summary of the global burden of low back and neck pain studies. Eur. Spine J. 586–17 (2018). doi:https://doi.org/10.1007/s00586-017-5432-9.
[3] GBD 2015 DALYs and HALE Collaborators, G. 2015 Daly. and H, Global, regional, and national disability-adjusted life-years (DALYs) for 315 diseases and injuries and healthy life expectancy (HALE), 1990–2015: a systematic analysis for the Global Burden of Disease Study 2015, Lancet (London, England) 388 (2016) 1603–1658.
[4] Dieleman, J. L. et al. US spending on personal health care and public health, 1996–2013. JAMA - J. Am. Med. Assoc. (2016). doi:https://doi.org/10.1001/jama.2016.16885.
[5] Brinjikji, W. et al. MRI findings of disc degeneration are more prevalent in adults with low back pain than in asymptomatic controls: a systematic review and meta-analysis. Am. J. Neuroradiol. 36, 2394–2399 (2015).
[6] C.H. Oh, S.H. Yoon, Whole spine disc degeneration survey according to the ages and sex using pfirrmann disc degeneration grades, Korean J. Spine 14 (2017) 148–154.
[7] J.A. Buckwalter, Aging and degeneration of the human intervertebral disc, Spine (Phila Pa 1976) 20 (1995) 1307–1314.
[8] Alini, M. et al. Are animal models useful for studying human disc disorders/degeneration? Eur. Spine J. 17, 2–19 (2008).
[9] J.C. Lotz, Animal models of intervertebral disc degeneration lessons learned, Spine (Phila Pa 1976) 29 (2004) 2742–2750.
[10] K. Singh, K. Masuda, H.S. An, Animal models for human disc degeneration, Spine J. 5 (2005) 267S–279S.
[11] G.E. Mosley, T.W. Evashwick-Rogler, A. Lai, J.C. Iatridis, Looking beyond the intervertebral disc: the need for behavioral assays in models of discogenic pain, Ann. N. Y. Acad. Sci. (2017), https://doi.org/10.1111/nyas.13429.
[12] J.C. Lotz, J.A. Ulrich, Innervation, inflammation, and hypermobility may characterize pathologic disc degeneration: review of animal model data, Journal of Bone and Joint Surgery - Series A 88 (2006) 76–82.
[13] Lipson, S. J. & Muir, H. 1980 Volvo award in basic science. Proteoglycans in experimental intervertebral disc degeneration. Spine (Phila Pa 1976). 6, 194–210 (1981).
[14] Lai, A. et al. Assessment of functional and behavioral changes sensitive to painful disc degeneration. J. Orthop. Res. 33, 755–64 (2015).
[15] Muralidharan, A. et al. Establishment and characterization of a novel rat model of mechanical low back pain using behavioral, pharmacologic and histologic methods. Front. Pharmacol. 8, 493 (2017).
[16] Kim, J.-S. et al. Development of an experimental animal model for lower back pain by percutaneous injury-induced lumbar facet joint osteoarthritis. J. Cell. Physiol. 230, 2837–2847 (2015).
[17] K. Omarker, R.R. Myers, Pathogenesis of sciatic pain: role of herniated nucleus pulposus and deformation of spinal nerve root and dorsal root ganglion, Pain 78 (1998) 99–105.
[18] K. Olmarker, B. Rydevik, T. Hansson, S. Holm, Compression-induced changes of the nutritional supply to the porcine cauda equina, J. Spinal Disord. 3 (1990) 25–29.
[19] S.J. Hu, J.L. Xing, An experimental model for chronic compression of dorsal root ganglion produced by intervertebral foramen stenosis in the rat, Pain (1998), https://doi.org/10.1016/S0304-3959(98)00067-0.
[20] X.-J. Song, S.-J. Hu, K.W. Greenquist, J.-M. Zhang, R.H. LaMotte, Mechanical and thermal hyperalgesia and ectopic neuronal discharge after chronic compression of dorsal root ganglia, J. Neurophysiol. 82 (1999) 3347–3358.
[21] Miyagi, M. et al. Assessment of pain behavior in a rat model of intervertebral disc injury using the catwalk gait analysis system. Spine (Phila Pa 1976). 38, 1459–1465 (2013).
[22] Li, Z. et al. Both expression of cytokines and posterior annulus fibrosus rupture are essential for pain behavior changes induced by degenerative intervertebral disc: an experimental study in rats. J. Orthop. Res. 32, 262–272 (2014).
[23] Onda, A. et al. Nerve growth factor content in dorsal root ganglion as related to changes in pain behavior in a rat model of experimental lumbar disc herniation. Spine (Phila Pa 1976). 30, 188–93 (2005).
[24] K. Ozawa, Y. Atsuta, T. Kato, Chronic effects of the nucleus pulposus applied to nerve roots on ectopic firing and conduction velocity, Spine (Phila Pa 1976) 26 (2001) 2661–2665.
[25] Suzuki, M. et al. Nuclear factor-kappa B decoy suppresses nerve injury and improves mechanical allodynia and thermal hyperalgesia in a rat lumbar disc herniation model. Eur. Spine J. 18, 1001–1007 (2009).
[26] Watanabe, K. et al. Increase of sodium channels (Nav 1.8 and Nav 1.9) in rat dorsal root ganglion neurons exposed to autologous nucleus pulposus. Open Orthop. J. 8, 69–73 (2014).
[27] R. Silberberg, M. Aufdermaur, J.H. Adler, Degeneration of the intervertebral disks and spondylosis in aging sand rats, Arch. Pathol. Lab. Med 103 (1979) 231–235.
[28] H.E. Gruber, T. Johnson, H.J. Norton, E.N. Hanley, The sand rat model for disc degeneration: radiologic characterization of age-related changes: cross-sectional and prospective analyses, Spine (Phila Pa 1976) (2002), https://doi.org/10.1097/00007632-200202010-00004.
[29] Gruber, H. E. et al. Brain-derived neurotrophic factor and its receptor in the human and the sand rat intervertebral disc. Arthritis Res. Ther. 10, R82 (2008).
[30] Kimura, T. et al. Progressive degeneration of articular cartilage and intervertebral discs. Int. Orthop. 20, 177–181 (1996).
[31] Allen, K. D. et al. Decreased physical function and increased pain sensitivity in mice deficient for type IX collagen. Arthritis Rheum. (2009). doi:https://doi.org/

10.1002/art.24783.
[32] Boyd, L. M. et al. Early-onset degeneration of the intervertebral disc and vertebral end plate in mice deficient in type IX collagen. Arthritis Rheum. (2008). doi:https://doi.org/10.1002/art.23231.
[33] Sahlman, J. et al. Premature vertebral endplate ossification and mild disc degeneration in mice after inactivation of one allele belonging to the Col2a1 gene for type II collagen. Spine (Phila Pa 1976). (2001). doi:https://doi.org/10.1097/00007632-200112010-00008.
[34] M. Millecamps, J.T. Czerminski, A.P. Mathieu, L.S. Stone, Behavioral signs of axial low back pain and motor impairment correlate with the severity of intervertebral disc degeneration in a mouse model, Spine J. 15 (2015) 2524–2537.
[35] M. Millecamps, M. Tajerian, L. Naso, E.H. Sage, L.S. Stone, Lumbar intervertebral disc degeneration associated with axial and radiating low back pain in ageing SPARC-null mice, Pain 153 (2012) 1167–1179.
[36] Miyagi, M. et al. ISSLS Prize winner: increased innervation and sensory nervous system plasticity in a mouse model of low back pain due to intervertebral disc degeneration. Spine (Phila Pa 1976). 39, 1345–54 (2014).
[37] Tajerian, M. et al. DNA methylation of SPARC and chronic low back pain. Mol. Pain 7, 65 (2011).
[38] M. Millecamps, M. Tajerian, E.H. Sage, L.S. Stone, Behavioral signs of chronic back pain in the SPARC-null mouse, Spine (Phila Pa 1976) 36 (2011) 95–102.
[39] Abdelaziz, D. M. et al. Behavioral signs of pain and functional impairment in a mouse model of osteogenesis imperfecta. Bone 81, 400–6 (2015).
[40] Lapveteläinen, T. et al. More knee joint osteoarthritis (OA) in mice after inactivation of one allele of type II procollagen gene but less OA after lifelong voluntary wheel running exercise. Osteoarthr. Cartil. 9, 152–160 (2001).
[41] Fässler, R. et al. Mice lacking alpha(IX) collagen develop noninflammatory degenerative joint disease. Proc. Natl. Acad. Sci. U. S. A. (1994). doi:https://doi.org/10.1073/pnas.91.11.5070.
[42] Mansergh, F. C. et al. Osteopenia in Sparc (osteonectin)-deficient mice: characterization of phenotypic determinants of femoral strength and changes in gene expression. Physiol. Genomics 32, 64–73 (2007).
[43] J.S. Mogil, S.E. Crager, What should we be measuring in behavioral studies of chronic pain in animals? Pain 112 (2004) 12–15.
[44] C.P. van Wilgen, R. Stewart, P.T. Patrick Stegeman, M. Coppes, M. van Wijhe, Fear of movement in pre-operative patients with a lumbar stenosis and or herniated disc: factor structure of the Tampa scale for kinesiophobia, Man. Ther. 15 (2010) 593–598.
[45] Winter, C. C. et al. Walking ability during daily life in patients with osteoarthritis of the knee or the hip and lumbar spinal stenosis: a cross sectional study. BMC Musculoskelet. Disord. 11, 233 (2010).
[46] J.H. Lee, J.H. An, S.H. Lee, I.S. Seo, Three-dimensional gait analysis of patients with weakness of ankle dorsiflexor as a result of unilateral L5 radiculopathy, J. Back Musculoskelet. Rehabil. 23 (2010) 49–54.
[47] Mitchell, K. et al. Differences in lumbar spine and lower extremity kinematics in people with and without low back pain during a step-up task: a cross-sectional study. BMC Musculoskelet. Disord. 18, 369 (2017).
[48] Masuda, K. et al. A novel rabbit model of mild, reproducible disc degeneration by an Anulus needle puncture: correlation between the degree of disc injury and radiological and histological appearances of disc degeneration. Spine (Phila Pa 1976). 30, 5–14 (2005).
[49] R.N. Walsh, R.A. Cummins, The open-field test: a critical review, Psychol. Bull. 83 (1976) 482–504.
[50] L. Steru, R. Chermat, B. Thierry, P. Simon, The tail suspension test: a new method for screening antidepressants in mice, Psychopharmacology 85 (1985) 367–370.
[51] S.M. Carlton, H.A. Lekan, S.H. Kim, J.M. Chung, Behavioral manifestations of an experimental model for peripheral neuropathy produced by spinal nerve ligation in the primate, Pain 56 (1994) 155–166.
[52] C. Yoon, Y. Young Wook, N. Heung Sik, K. Sun Ho, C. Jin Mo, Behavioral signs of ongoing pain and cold allodynia in a rat model of neuropathic pain, Pain 59 (1994) 369–376.
[53] M. Fitzgerald, Capsaicin and sensory neurones — a review, Pain 15 (1983) 109–130.
[54] S.A. Malin, B.M. Davis, D.C. Molliver, Production of dissociated sensory neuron cultures and considerations for their use in studying neuronal function and plasticity, Nat. Protoc. 2 (2007) 152–160.
[55] Hartvigsen, J. et al. What low back pain is and why we need to pay attention. Lancet (London, England) 0, (2018).
[56] de Schepper, E. I. T. et al. The association between lumbar disc degeneration and low back pain. Spine (Phila Pa 1976). 35, 531–536 (2010).
[57] D.M. Elliott, J.J. Sarver, Young investigator award winner: validation of the mouse and rat disc as mechanical models of the human lumbar disc, Spine (Phila Pa 1976) 29 (2004) 713–722.
[58] G.D. O'Connell, E.J. Vresilovic, D.M. Elliott, Comparison of animals used in disc research to human lumbar disc geometry, Spine (Phila Pa 1976) (2007), https://doi.org/10.1097/01.brs.0000253961.40910.c1.
[59] T. Winkler, E.J. Mahoney, D. Sinner, C.C. Wylie, C.L. Dahia, Wnt signaling activates Shh signaling in early postnatal intervertebral discs, and re-activates Shh signaling in old discs in the mouse, PLoS One 9 (2014).
[60] B. Vernon-Roberts, R.J. Moore, R.D. Fraser, The natural history of age-related disc degeneration, Spine (Phila Pa 1976) 33 (2008) 2767–2773.
[61] O. Alvarez-Garcia, T. Matsuzaki, M. Olmer, K. Masuda, M.K. Lotz, Age-related reduction in the expression of FOXO transcription factors and correlations with intervertebral disc degeneration, J. Orthop. Res. (2017), https://doi.org/10.1002/jor.23583.
[62] David, G., Ciurea, a V, Iencean, S. M. & Mohan, A. Angiogenesis in the degeneration of the lumbar intervertebral disc. J. Med. Life 3, 154–161 (2010).
[63] M.H. Coppes, E. Marani, R.T. Thomeer, G.J. Groen, Innervation of 'painful' lumbar discs, Spine (Phila Pa 1976) 22 (1997) 2342–2349 discussion 2349-50.
[64] S.M. Albelda, W.A. Muller, C.A. Buck, P.J. Newman, Molecular and cellular properties of PECAM-1 (endoCAM/CD31): a novel vascular cell-cell adhesion molecule, J. Cell Biol. 114 (1991) 1059–1068.
[65] Wilkinson, K. D. et al. The neuron-specific protein PGP 9.5 is a ubiquitin carboxyl-terminal hydrolase. Science. (1989). doi:https://doi.org/10.1126/science.2530630.
[66] C. Kent, P.J. Clarke, The immunolocalisation of the neuroendocrine specific protein PGP9.5 during neurogenesis in the rat, Dev. Brain Res. 58 (1991) 147–150.
[67] T.L. Kelly, K.E. Wilson, S.B. Heymsfield, Dual energy X-ray absorptiometry body composition reference values from NHANES, PLoS One 4 (2009) e7038.
[68] J.R. Deuis, L.S. Dvorakova, I. Vetter, Methods used to evaluate pain behaviors in rodents, Front. Mol. Neurosci. 10 (2017).
[69] Spijker-Huiges, A. et al. Radiating low back pain in general practice: incidence, prevalence, diagnosis, and long-term clinical course of illness. Scand. J. Prim. Health Care 33, 27–32 (2015).
[70] K. Konstantinou, K.M. Dunn, Sciatica: review of epidemiological studies and prevalence estimates, Spine (Phila Pa 1976) 33 (2008) 2464–2472.
[71] Julius, D. et al. The capsaicin receptor: a heat-activated ion channel in the pain pathway. Nature 389, 816–824 (1997).
[72] Moparthi, L. et al. Human TRPA1 is intrinsically cold- and chemosensitive with and without its N-terminal ankyrin repeat domain. Proc. Natl. Acad. Sci. U. S. A. 111, 16901–6 (2014).
[73] J.E. Swett, Y. Torigoe, V.R. Elie, C.M. Bourassa, P.G. Miller, Sensory neurons of the rat sciatic nerve, Exp. Neurol. 114 (1991) 82–103.
[74] M. Renganathan, T.R. Cummins, S.G. Waxman, Contribution of Na_v 1.8 sodium channels to action potential electrogenesis in DRG neurons, J. Neurophysiol. 86 (2001) 629–640.
[75] Maingret, F. et al. Inflammatory mediators increase Nav1.9 current and excitability in nociceptors through a coincident detection mechanism. J. Gen. Physiol. 131, 211–25 (2008).
[76] D.I. Rubin, Epidemiology and risk factors for spine pain, Neurol. Clin. 25 (2007) 353–371.
[77] Boos, N. et al. Classification of age-related changes in lumbar intervertebral discs. Spine (Phila Pa 1976). 27, 2631–2644 (2002).
[78] M.V. Risbud, I.M. Shapiro, Role of cytokines in intervertebral disc degeneration: pain and disc content, Nat. Rev. Rheumatol. 10 (2013) 44–56.
[79] Z.I. Johnson, Z.R. Schoepflin, H. Choi, I.M. Shapiro, M.V. Risbud, Disc in flames: roles of TNF-α and IL-1β in intervertebral disc degeneration, Eur. Cell. Mater. 30 (2015) 104–116 discussion 116–7.
[80] C.L. Le Maitre, J.A. Hoyland, A.J. Freemont, Catabolic cytokine expression in degenerate and herniated human intervertebral discs: IL-1β and TNFα expression profile, Arthritis Res. Ther. (2007), https://doi.org/10.1186/ar2275.
[81] C.L. Le Maitre, A.J. Freemont, J.A. Hoyland, The role of interleukin-1 in the pathogenesis of human intervertebral disc degeneration, Arthritis Res. Ther. (2005), https://doi.org/10.1186/ar1732.
[82] Bachmeier, B. E. et al. Analysis of tissue distribution of TNF-α, TNF-α-receptors, and the activating TNF-α-converting enzyme suggests activation of the TNF-α system in the aging intervertebral disc. in Ann. N. Y. Acad. Sci. (2007). doi:https://doi.org/10.1196/annals.1397.069.
[83] Hayashi, S. et al. TNF-alpha in nucleus pulposus induces sensory nerve growth a study of the mechanism of discogenic low back pain using tnf-alpha-deficient mice. Spine (Phila Pa 1976). (2008). doi:https://doi.org/10.1097/BRS.0b013e318178e5ea.
[84] Lee, J. M. et al. Interleukin-1β induces angiogenesis and innervation in human intervertebral disc degeneration. J. Orthop. Res. (2011). doi:https://doi.org/10.1002/jor.21210.
[85] Andrade, P. et al. Tumor necrosis factor-α levels correlate with postoperative pain severity in lumbar disc hernia patients: opposite clinical effects between tumor necrosis factor receptor 1 and 2. Pain (2011). doi:https://doi.org/10.1016/j.pain.2011.08.012.
[86] Andrade, P. et al. Elevated levels of tumor necrosis factor-α and TNFR1 in recurrent herniated lumbar discs correlate with chronicity of postoperative sciatic pain. Spine J. (2016). doi:https://doi.org/10.1016/j.spinee.2015.10.038.
[87] Nasto, L. A. et al. ISSLS prize winner: inhibition of NF-κB activity ameliorates age-associated disc degeneration in a mouse model of accelerated aging. Spine (Phila Pa 1976). 37, 1819–25 (2012).
[88] K. Akeda, T. Yamada, N. Inoue, A. Nishimura, A. Sudo, Risk factors for lumbar intervertebral disc height narrowing: a population-based longitudinal study in the elderly, BMC Musculoskelet. Disord. 16 (2015) 344.
[89] G. Hassett, D.J. Hart, N.J. Manek, D.V. Doyle, T.D. Spector, Risk factors for progression of lumbar spine disc degeneration: the Chingford study, Arthritis Rheum. 48 (2003) 3112–3117.
[90] Lavsky-Shulan, M. et al. Prevalence and functional correlates of low back pain in the elderly: the Iowa 65+ Rural Health Study. J. Am. Geriatr. Soc. 33, 23–8 (1985).
[91] M. Higuchi, K. Abe, K. Kaneda, Changes in the nucleus pulposus of the intervertebral disc in bipedal mice. A light and electron microscopic study, Clin. Orthop. Relat. Res. (1983) 251–257.
[92] W.B. Ershler, E.T. Keller, Age-associated increased interleukin-6 gene expression, late-life diseases, and frailty, Annu. Rev. Med. 51 (2000) 245–270.
[93] R.P. Stowe, M.K. Peek, M.P. Cutchin, J.S. Goodwin, Plasma cytokine levels in a population-based study: relation to age and ethnicity, Journals Gerontol. Ser. A Biol. Sci. Med. Sci. 65A (2010) 429–433.

[94] Bair, W.-N. et al. Of aging mice and men: gait speed decline is a translatable trait, with species-specific underlying properties. Journals Gerontol. Ser. A (2019). doi:https://doi.org/10.1093/gerona/glz015.
[95] Justice, J. N. et al. Battery of behavioral tests in mice that models age-associated changes in human motor function. Age (Omaha). (2014). doi:https://doi.org/10.1007/s11357-013-9589-9.
[96] A. Fahlström, Q. Yu, B. Ulfhake, Behavioral changes in aging female C57BL/6 mice, Neurobiol. Aging 32 (2011) 1868–1880.
[97] Houtkooper, R. H. et al. The metabolic footprint of aging in mice. Sci. Rep. (2011). doi:https://doi.org/10.1038/srep00134.
[98] M.L. Ferreira, A. McLachlan, The challenges of treating sciatica pain in older adults, Drugs Aging 33 (2016) 779–785.
[99] J.-A. Zwart, T. Sand, Repeatability of dermatomal warm and cold sensory thresholds in patients with sciatica, Eur. Spine J. 11 (2002) 441–446.
[100] Mahn, F. et al. Sensory symptom profiles and co-morbidities in painful radiculopathy. PLoS One 6, e18018 (2011).
[101] B. Tampin, N.K. Briffa, H. Slater, Self-reported sensory descriptors are associated with quantitative sensory testing parameters in patients with cervical radiculopathy, but not in patients with fibromyalgia, Eur. J. Pain 17 (2013) 621–633.
[102] O.P. Nygaard, S.I. Mellgren, The function of sensory nerve fibers in lumbar radiculopathy. Use of quantitative sensory testing in the exploration of different populations of nerve fibers and dermatomes, Spine (Phila Pa 1976) 23 (1998) 348–352 discussion 353.
[103] King-Himmelreich, T. et al. Age-dependent changes in the inflammatory nociceptive behavior of mice. Int. J. Mol. Sci. 16, 27508–27519 (2015).
[104] C.J. Laedermann, H. Abriel, I. Decosterd, Post-translational modifications of voltage-gated sodium channels in chronic pain syndromes, Front. Pharmacol. 6 (2015).
[105] Wu, D.-F. et al. PKCε phosphorylation of the sodium channel NaV1.8 increases channel function and produces mechanical hyperalgesia in mice. J. Clin. Invest. 122, 1306–15 (2012).